Journal of Materials Processing Tech. 251 (2018) 241–250

Contents lists available at ScienceDirect

Journal of Materials Processing Tech.

journal homepage: www.elsevier.com/locate/jmatprotec

Weld-bonded stainless steel to carbon fibre-reinforced plastic joints

Adam M. Joesbury[a,c], Paul A. Colegrove[a,*], Patrick Van Rymenant[b], David S. Ayre[a], Supriyo Ganguly[a], Stewart Williams[a]

[a] College Road, Cranfield, Bedfordshire MK43 0AL, UK
[b] KU Leuven, Mechanical Engineering Technology TC, Jan De Nayerlaan 5, 2860 Sint-Katelijne-Waver, Belgium
[c] The University of Manchester, Oxford Rd, Manchester M13 9PL, UK

ARTICLE INFO

Keywords:
Composite metal joining CFRP weld-bonding spot-welding

ABSTRACT

This paper investigates a resistance spot welded reinforced adhesive (weld-bonded) joint between 304 stainless steel to carbon fibre reinforced plastic (CFRP), where welds are made both with and without the reinforcing carbon fibres present. Successful welds with the fibres present could only be produced with high electrode pinch forces, which helped reduce contamination of the weld nugget. Similar joint strengths were achieved in both cases, however the joints without fibres exhibited an increased strain to failure. Both joints were significantly stronger than either an adhesive joint or a comparable bolt reinforced adhesive joint. These techniques provide an alternative for joining thin metallic components to CFRP structures where increased strength and integrity is required.

1. Introduction

The subject of composite metal joining has received increasing attention in recent years because of the desire to obtain optimised properties at different locations of a structure. In many applications the introduction of composites can contribute to an overall weight saving, however joints with the metallic structure are challenging.

Bolting can be used, but they lead to significant stress concentrations around the bolt holes and add weight. Breto et al. (2015) stated that adhesively bonded joints can overcome these shortcomings, have high structural integrity and improved corrosion performance. However the stress concentrates at the end of the bond-line causing failure which is often catastrophic. The performance may be improved by 70% by grading the properties of the adhesive.

Zhang et al. (2012) stated that the limitations of bolted and adhesively bonded joints are addressed by combining the two processes, however this often defeats the original objective of size, weight and cost savings. Therefore several techniques have been developed that involve creating features on the metallic part to reinforce the joint. This includes the Comeld process which uses an electron beam to create features on the metal surface that improve strength. Similar work by Ucsnik et al. (2010) used a Metal Inert Gas based welding process called Cold Metal Transfer to create pins that had a variety of shapes including balls that helped prevent pull-out. These joints prevented the catastrophic failure of the adhesive only joints, dramatically increasing the strain to failure. There are a large number of publications that investigate pin failure and pull out with a good recent article being published by Nguyen et al. (2017). In this article the pins were manufactured via an additive manufacture technique, Selective Laser Melting, and surface features on the pins were added to improve energy absorption by 60%.

Weld bonding, which is the subject of this study, was first reported by Schwartz (1979) who stated that it had been developed for metal to metal joints in the USSR and it combined a resistance spot weld (RSW) with adhesive bonding. Darwish and Ghanya (2000) describe how two variants of the process have been developed: weld-through and back-infiltration. In the weld-through process an adhesive is applied to faying surfaces. The surfaces are then brought together and a RSW is applied prior to adhesive cure so the weld penetrates the adhesive layer. In the back-infiltration process metal parts are directly joined by resistance spot welding followed by the application of a low viscosity adhesive to the edge of the overlap, which fills the gap by capillary action. The method has a number of advantages over mechanical fastening including reduced manufacturing costs, high static and fatigue strengths, and improved corrosion performance. Subsequent finite element modelling of weld-bonded joints by Al-Samhan and Darwish (2003) demonstrated how incorporating the RSW with the weld-bonded joint distributed the stresses over a wider area, increasing the overall strength. Santos et al. (2004) conducted a thorough study on weld-bonded joints and used a finite element code, SORPAS to model the

* Corresponding author.
E-mail address: p.colegrove@cranfield.ac.uk (P.A. Colegrove).

http://dx.doi.org/10.1016/j.jmatprotec.2017.08.023
Received 6 April 2017; Received in revised form 25 July 2017; Accepted 18 August 2017
Available online 24 August 2017

resistance spot welding process and understand the effect of the adhesive. Mechanical tests were undertaken to assess performance, demonstrating the synergistic effect of weld-bonding which provided a greater displacement to failure than either spot welding or adhesive bonding on their own.

More recently these techniques have been applied to joints between metals and composites. Berger (2010) demonstrated joints where the fibres were removed at the locations that the resistance spot welds were applied. Shah et al. (2010) produced similar joints and showed that the load carrying capacity of the weld-bonded joint was similar. However failure of these joints was less catastrophic as the spot weld continued to provide strength after failure of the adhesive. Furthermore the fatigue strength of the joints was improved and once again failure when it occurred was less catastrophic. The most recent work on these kinds of joints by Li and Sun (2014) involved numerical modelling of joint performance and predicted the failure modes as a function of the adhesive layer thickness. In addition, they investigated the effect of impact damage on joint strength.

Joesbury (2016) extended the weld-bonding method showing how the RSW could be made *through* the carbon fibre fabric. A diagram of the joint investigated is shown in Fig. 1. This joint has an interleaved stack of metal and dry carbon fibre across which a RSW is made. The fibres are partially expelled and partially absorbed into the metallic welded joint. A number of metals were compared and stainless steel was shown to be more effective than either titanium or aluminium. The most successful joints with this metal used three layers of 0.9 mm thick stainless steel between 2 × 2 plies of carbon fibre fabric. The small metal sheet in the middle has the same area as the bonded interface and is critical to the success of the joint. As will be demonstrated within this paper, the resistance of the layup scales with the number of fibre to metal interfaces. Hence the addition of the middle sheet creates more heat and facilitates absorption of the fibres within the weld metal. The second stage involved epoxy resin infusion into the carbon fibre fabric. The resin has two functions, it forms the polymer matrix system of the composite laminate and also an adhesive joint between the composite laminate and metal.

This paper describes the effect of process parameters on the RSW process. This is followed by the design and manufacture of proof of concept joints that were mechanically tested to determine joint performance.

2. Methodology

2.1. Equipment

The welds require accurate control of the electrode pinch force. To achieve this, an AWL-Techniek WP63RL-K resistance spot welder was used where the upper electrode was pneumatically actuated (max load 4.5 kN). This equipment is shown in Fig. 2 as well as the arrangement of the weld and a small tent enclosure that was filled with argon to minimise oxidation of the metal and combustion of the fibres during welding. The oxygen concentration was kept below 500 ppm. The copper electrodes had a contact diameter of 3.5 mm and were dressed regularly on any sign of wear or contamination to ensure consistent welds. The welding machine was instrumented in a number of ways: a calibrated inline pressure transducer; current and voltage probes; and a Polytec CLV-1000 Laser vibrometer to measure electrode displacement. All these devices were connected to a Dewetron DEWE-2600 data logger.

2.2. Parametric weld study

The parametric weld study was conducted to determine optimum resistance spot welding parameters for the interleaved material stack shown in Fig. 1, i.e. a weld was created between three sheets of 0.9 mm thick 304L stainless steel and 2 × 2 ply sheets of 0.25 mm Hexcel G1157 carbon fibre fabric which was laid up in a 0°/0° orientation. The size of the middle metal sheet was the same as the bonded interface – 30 × 30 mm and the combined thickness of the joint was 3.7 mm.

To determine appropriate parameters for this study, the through thickness resistivity needed to be determined as a function of the electrode pinch force. A Sensy INDI-PSD handheld force transducer indicator together with a 9QUAL 10 kN load cell was used to measure pinch force and a Master Instruments D3700 micro ohmmeter was used to measure electrical resistance. The following material stacks were investigated:

- Metal to metal – 0.9 mm 304L stainless steel/0.9 mm 304L stainless steel
- Multi-material stack 1–0.9 mm 304L stainless steel/1x Hexcel G1157 carbon fibre fabric ply/0.9 mm 304L stainless steel
- Multi-material stack 2–0.9 mm 304L stainless steel/2x Hexcel G1157 carbon fibre fabric plies/0.9 mm 304L stainless steel/2x Hexcel G1157 carbon fibre fabric plies/0.9 mm 304L stainless steel

Fig. 3 shows the measured through-the-thickness resistivity as a function of the pinch force. In all cases an increasing pinch force resulted in a reduced resistance, which asymptotes to a particular value that corresponds to flattening of the surface asperities with metal to metal contact and increased nesting density of the carbon fibre for the multi-material stacks.

The dominant characteristic that affects the resistivity appears to be the number of carbon fibre to metal interfaces: there is only *one* ply and two interfaces in multi-material stack 1 (red square data points); while there are *four* plies and four interfaces in the multi-material stack 2 (blue circle data points). Since the resistivity is approximately doubled and the resistivity of stainless steel is relatively low, it would appear to scale with the number of interfaces.

Using this information, four series of experiments were performed on the interleaved material stack (Fig. 1) and the parameters are summarised in Fig. 4 the main parameters that were varied were the welding power, and the electrode pinch force. The current application time was varied during the experiments, but generally had a small effect once a weld has been made. Values between 1.3 and 2 s were used.

Series 1 trialled various power levels while keeping the electrode pinch force constant at 1990 N – the asymptote for multi-material

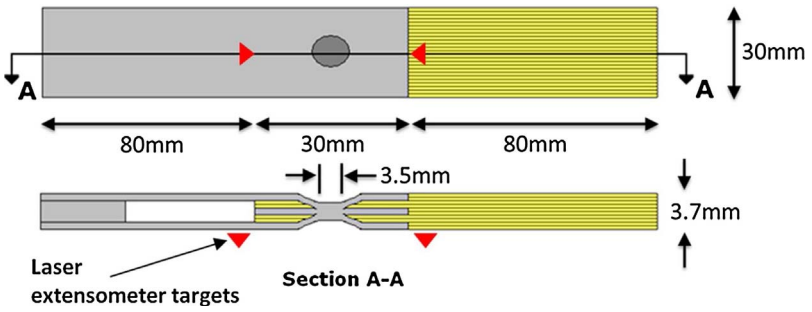

Fig. 1. Diagram of the metal to carbon fibre spot weld-braze reinforced adhesive joint. Note: this diagram shows the preferred interleaved stacking sequence.

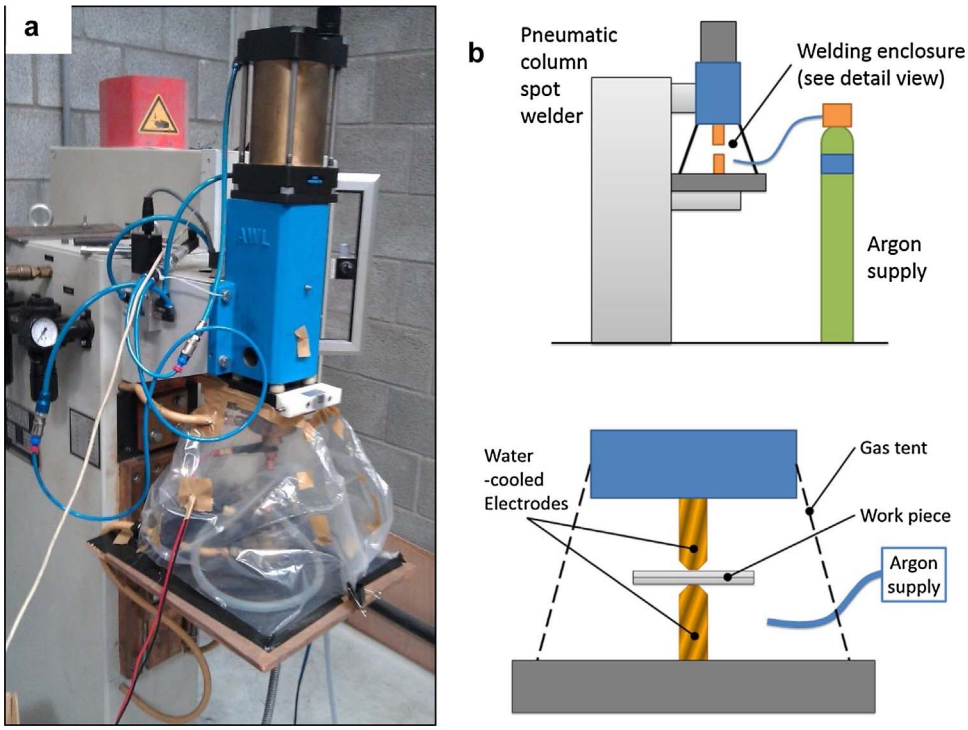

Fig. 2. (a) Photo and (b) schematic diagrams of AWL-Techniek WP63RL-K resistance spot welder, with gas enclosure tent around electrodes.

stack 2 in Fig. 3. For Series 2; electrode pinch force was increased to 3010 N and maintained for trials of various power levels. For Series 3; the power setting was kept constant at 15.7 kVA and the electrode pinch force was increased to above 4.5 kN. Series 4 was conducted at the second highest force to investigate whether further weld formation improvements could be achieved with higher power levels.

2.3. Test specimen manufacture and testing

A total of six mechanical test specimen types were manufactured for lap shear testing, which are summarised in Table 1. The six specimen types were created to understand the individual contributions from the adhesive joint, and the weld with and without fibres. The first test specimen involved an adhesive only joint without any weld and was used as a reference. Two joints were then created with and without fibres at the weld interface, and without any adhesive bond between the fibres and the stainless steel. This was achieved by placing PTFE release film at the interfaces to prevent adhesion between the stainless steel and the resin. These joints were manufactured to test the strength of the weld alone. The specimens without fibres were manufactured by cutting 9.5 × 9.5 mm square holes in the carbon fibre fabric, using embroidery scissors, the holes aligned with the position of where the weld was created.

Two comparative joints (i.e. welds with and without fibres) were then created without release film to test the combined strength of the welds with the adhesive bond. Finally, one joint was created with a bolted connection to test the conventional method for creating such a joint. The bolt had a similar diameter to the resistance spot weld.

The resistance spot welds with the fibres were created with the parameters indicated in the circle in Fig. 4, and are summarised in Table 2. The layup sequence, materials and fabric were identical to those used in the parametric study in Section 2.2. The parameters for the welds without the fibres were easier to produce and are also shown in Table 2 the main difference was the much shorter duration 0.3 s and

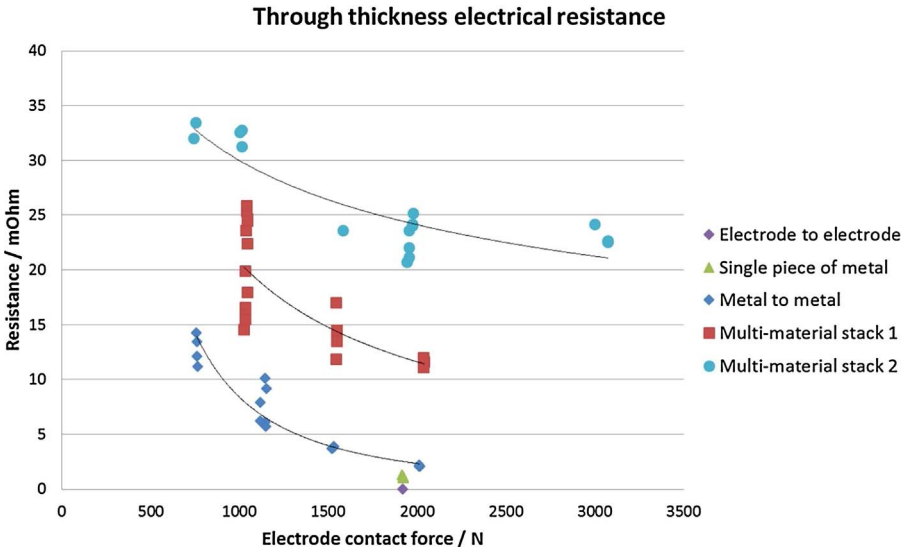

Fig. 3. Through thickness resistivity as a function of the electrode clamp force.

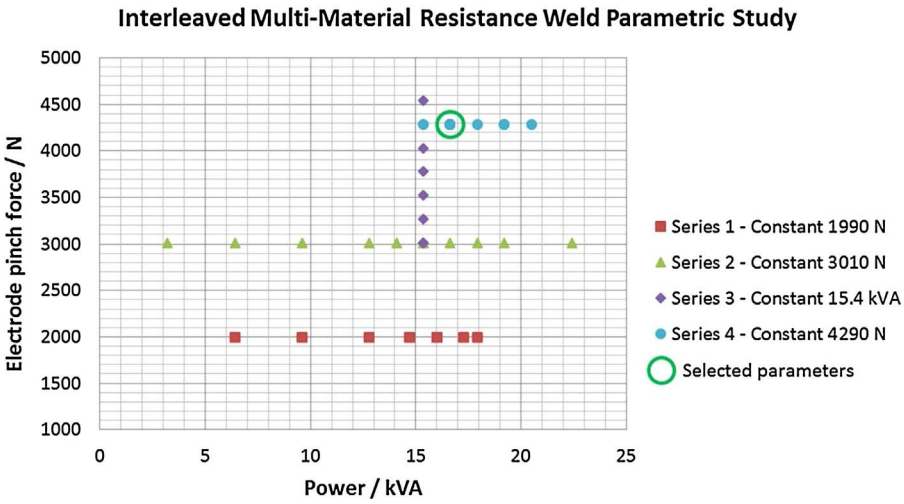

Fig. 4. RSW parameters investigated in the Interleaved Multi Material spot weld joints.

Table 1
Summary of mechanical test specimens.

Structural configuration	Adhesive bond	Weld	Fibres at weld
Adhesive bond only 	Yes	No	N/A
Weld (fibres) only 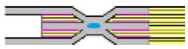	No	Yes	Yes
Weld (no fibres) only 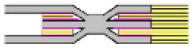	No	Yes	No
Weld (fibres) and adhesive bond 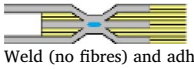	Yes	Yes	Yes
Weld (no fibres) and adhesive bond 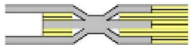	Yes	Yes	No
Adhesive bond reinforced with a mechanical fastener 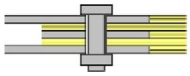	Yes	No	N/A

the higher power used.

The sequential steps to resin infuse the sample ready for lap shear testing are illustrated in Fig. 5. After creating the weld, additional plies of carbon fibre fabric were inserted in between the plies connected to the metal sheets (right hand side) and an insert was placed in between the two metal sheets (left hand side).

The whole assembly was then infused with RTM6 epoxy resin using a vacuum assisted resin transfer technique. RTM6 was chosen due to its wide use and well understood behaviour, and the relatively low viscosity when at infusion temperatures of 120 °C. This ensured good penetration into the interleaved stack area, including the weld site. The test specimens were infused in batches. Seven specimens were cured in each batch; with specimens of each test configuration being cured in each batch, reducing the possibility of introducing a systematic error for any individual test specimen configuration. Seven specimens of each joint type were produced so to ensure that at least five mechanical test results were obtained for each. Vacuum infusion was carried out using preheated (80 °C) and degassed RTM6 epoxy resin. Specimens and tooling were preheated to 120 °C and temperature maintained during infusion. After complete wet-out of the carbon fibre plies the resin was cured at 160 °C for 2 h.

One specimen was micro-sectioned, to check that the resin had fully infused both the fibre fabric and weld region, validating the resin infusion process.

The test specimens were prepared by adhesive bonding aluminium tabs to the composite laminate in the area that was to be clamped in the test rig. Laser extensometer reflective strips were applied at the boundaries of the joint interface, as shown in Fig. 1. Mechanical testing was performed using an Instron 5500/6025 test frame operating with a 100 kN load cell at a cross-head displacement speed of 1 mm/min.

2.4. Metallographic inspection

The specimens were sectioned through the weld nugget both parallel and perpendicular to the fibres. To observe microstructure detail in the weld nugget specimens were etched with Kalling's No. 1 etchant. The etchant was applied to the polished surfaces using a cotton wool swab for an expose time of 10 s followed by rinsing in flowing water for up to 30 s.

3. Results and discussion

3.1. Parametric study of welds with fibres

The series 1 welds, Fig. 3, were performed at an electrode pinch force of 1990N, corresponding to the start of the asymptote in resistivity (Fig. 3). These welds were of poor quality and either fell apart or could be easily separated by hand. In this case the load was insufficient to displace the fibres and produce a well-formed weld nugget.

For the series 2 and 4 welds the electrode pinch force was increased

Table 2
Summary of parameters used to manufacture the resistance spot welds in the test specimens.

Type of weld	Pinch force		Electric current		Weld time	
	Measured pneumatic pressure	Exerted force	% of equipment maximum power	Measured peak current	Number of cycles	Actual time
Weld with fibres	5.2 bar	4.29 kN	26% (16.6 kVA)	7.68 kA	65 @ 50 Hz	1.30 s
Weld without fibres	5.2 bar	4.29 kN	40% (25.6 kVA)	11.8 kA	15 @ 50 Hz	0.30 s

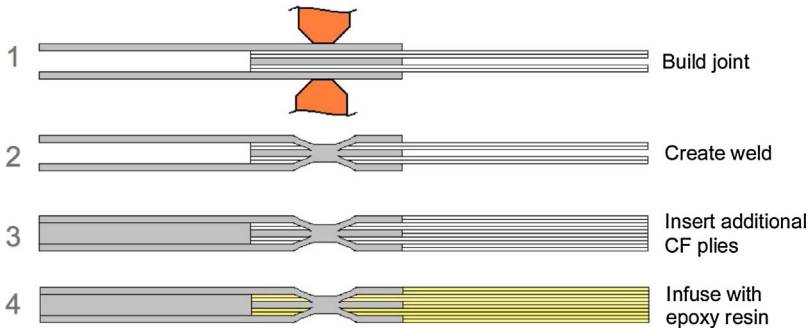

Fig. 5. Schematic diagram summarising the manufacture of the test specimens.

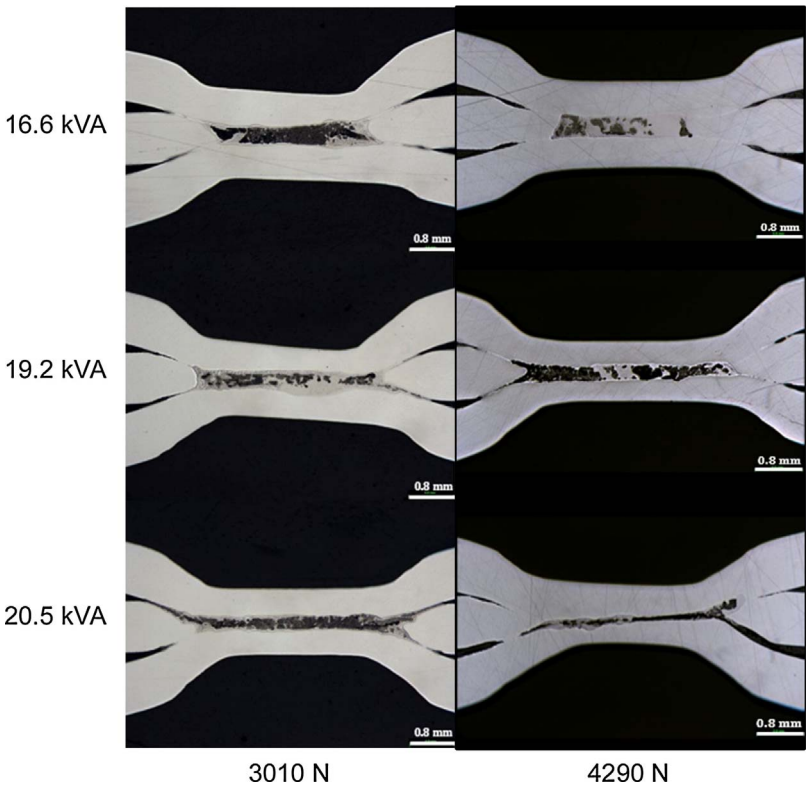

Fig. 6. Macrosections showing the effect of both the electrode pinch force and increasing power (current).

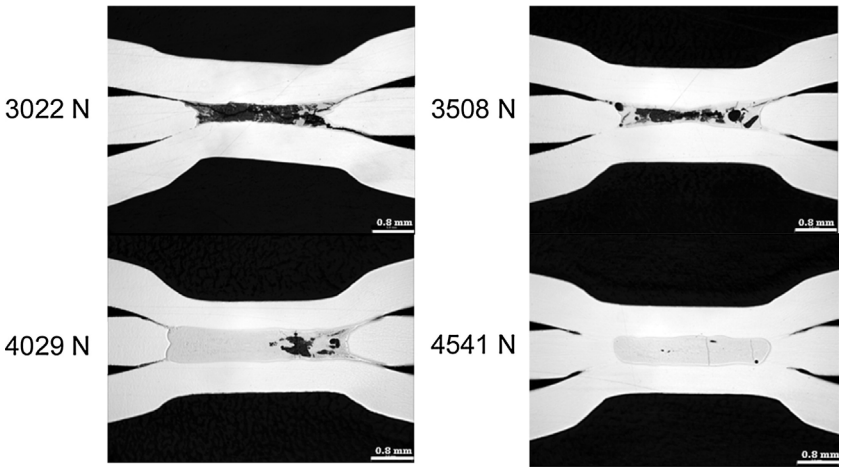

Fig. 7. Macrosections showing the effect of increasing electrode pinch force with a constant welding electrical power of 15.4 kVA.

to 3010N and 4290N respectively. Macrosections from welds are presented in Fig. 6. No consolidated welds were produced at low power, however when the power was increased to 15.4 kVA the parts were sufficiently joined to prevent them being easily separated by hand. As the power level increased further, there was an increase in weld splash from between interleaved layers; a thinning of the stainless steel sheets; and a widening of the weld nugget due to the increased power. There was no increase in the quality of the weld nugget formation as assessed

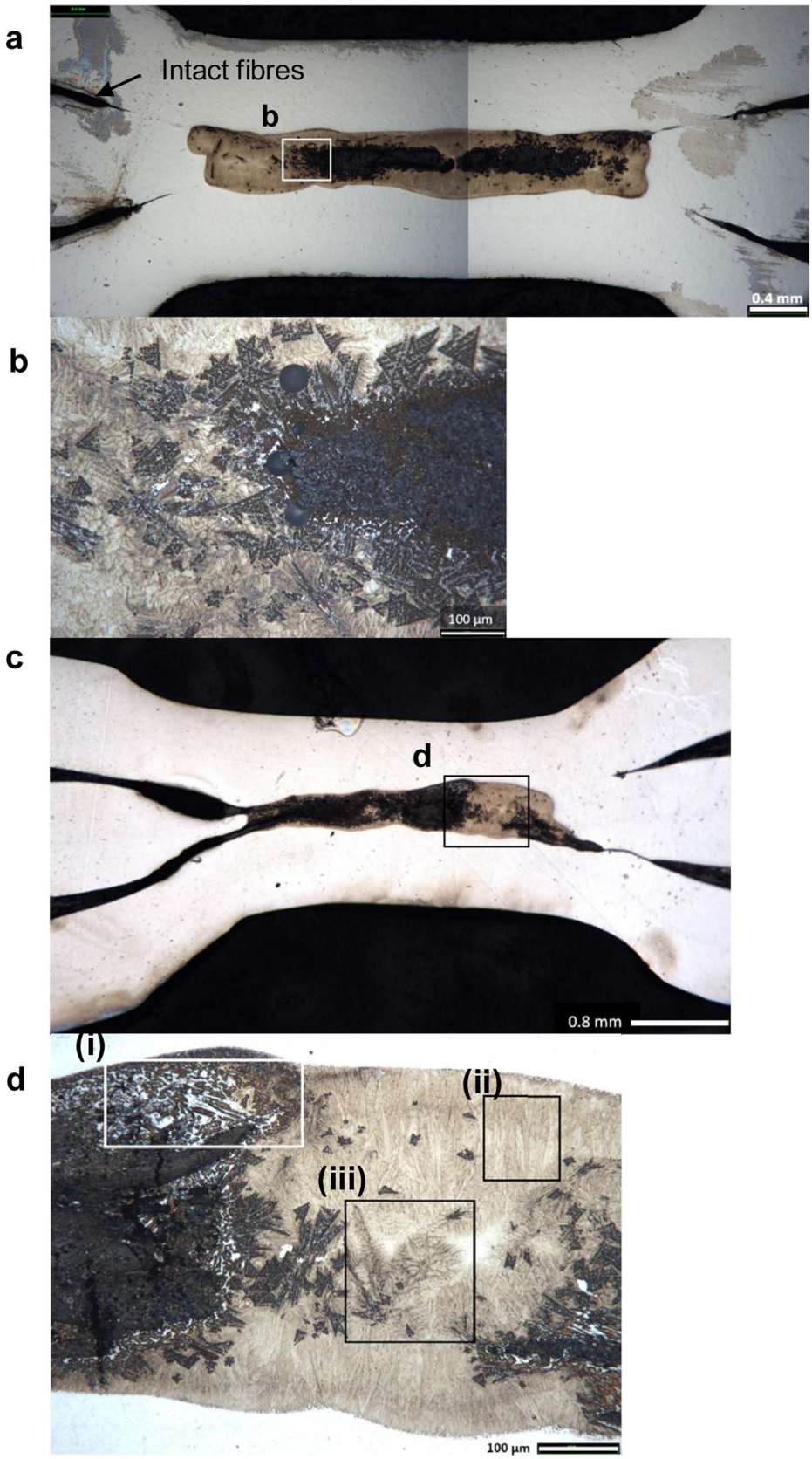

Fig. 8. (a) Fibre transverse macrostructure from 4290 N, 16.6 kVA weld; and (b) enlarged microstructure. (c) longitudinal macrostructure; and (d) enlarged microstructure.

by whether remnants of the fibres are present and consolidation of the weld nugget. These effects were not time dependent – there was little change once a joint had been formed. Increasing the load resulted in an improvement in the weld quality with minimal effect on the substrate thinning. The sample manufactured with a power of 16.6 kVA provided a good balance between weld nugget formation and substrate thinning and was therefore selected for the metal composite joints tested in a subsequent section.

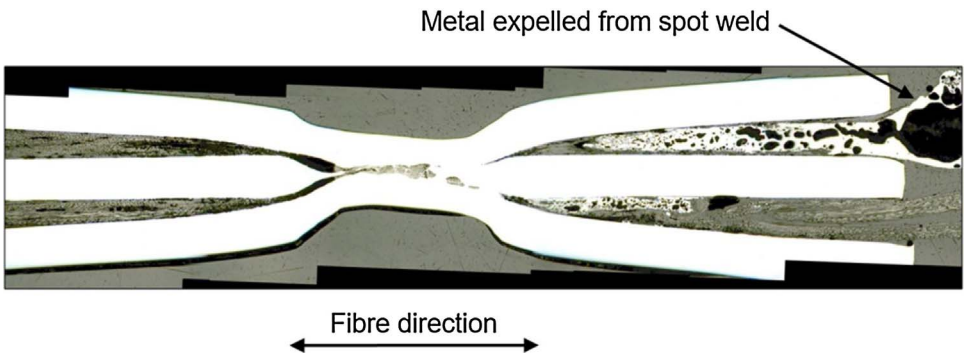

Fig. 9. Macrosection showing flow of molten metal that has been expelled from the spot weld nugget formation region. This weld was produced with a force of 4290 N and a power of 16.6 kVA.

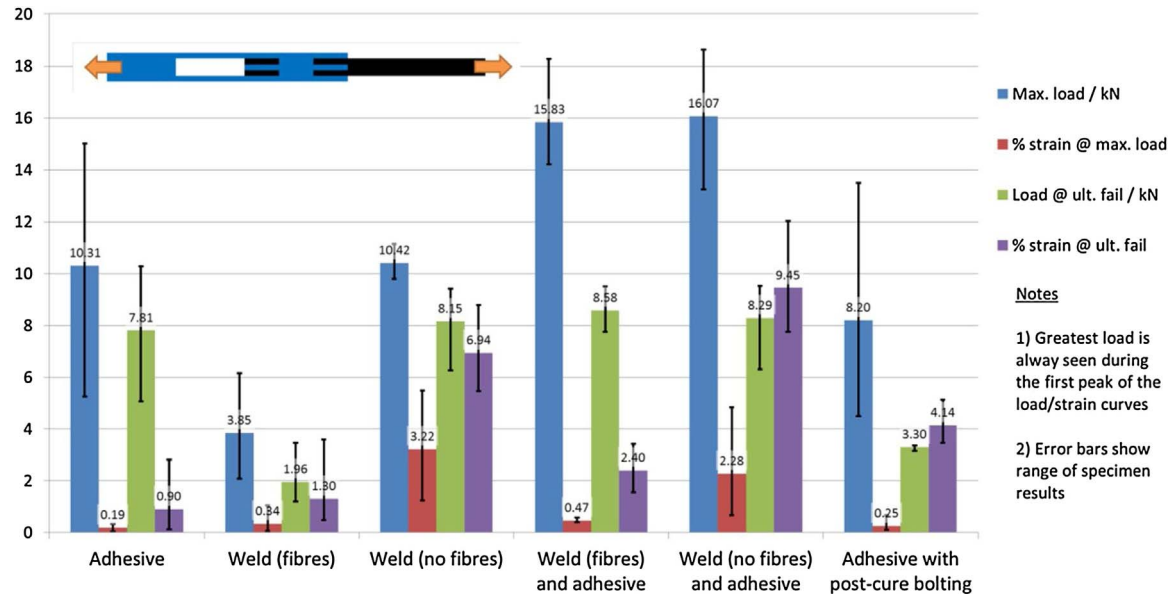

Fig. 10. Summary of strength performance of the different joint types (values are averaged for 5 test samples for each type).

Table 3
Lap joint failure mechanisms.

Joint	Failure mechanism	Comment
Adhesive	Mixed Cohesive/Adhesive failure (Fig. 11(a))	Peel promotes initial adhesive failure.
Weld(fibres)	Weld fails at centre and joint peels apart (Fig. 11(b))	Composite adherend remains complete except for region that failed around weld.
Weld(no fibres)	Weld intact, fail of composite by shear-out (Fig. 11(c))	Peel forces cause steel adherend run-outs to distort.
Weld(fibres) + Adhesive	Adhesive failure followed by weld failure (Fig. 12(a))	Weld reduces peel. Adhesive fails and load transfers to the weld nugget.
Weld(no fibres) + Adhesive	Two failure mechanisms:	
	Adhesive joint fail followed by composite shear-out (Fig. 12(b))	Weld connecting steel parts remains intact
	Adhesive failure at surfaces (not insert) and weld fails by ductile tearing (Fig. 12(c))	Weld nugget remains intact and torn from steel adherends − centre steel remains bonded.
Adhesive + Bolt	Adhesive failure followed by shear failure of bolt	No synergistic effects

The positive benefit of increasing the electrode pinch force was explored further with series 3 and the macrosections are shown in Fig. 7. The weld that was formed with a 4540N pinch force was particularly high quality with very few remnants of fibre being visible within the weld nugget. The increase in force aids expulsion of the fibres from the joint region enabling the formation of a nugget with minimal defects. This load was not explored further because it was at the limit of the welding equipment used.

3.2. Weld microstructure

Fig. 8(a,c) show the macrosections from the weld; with the weld nugget being the brown rectangular region. Traditionally, resistance spot welds have an oval shape, however the geometry of two interfaces and the presence of the fibres result in the rectangular shape. Some of the fibres remain intact and can only be seen outside the weld area as shown in the figure. Within the centre of the nugget there is a large black region which constitutes the remnants of the fibres.

The microstructure illustrated in Fig. 8(b,d) clearly shows a graded structure with carbon content varying from the vicinity of the fibres to a lower value nearer to the stainless steel boundary. This resulted in graphitisation of carbon where sufficient carbon diffusion occurred within molten stainless steel weld pool. The molten behaviour of stainless steel can be seen in dendritic structures as depicted in areas (ii) & (iii) within Fig. 8(d). Depending on the relative concentration of carbon in the graded structure, Iijima (1980) found that it can be

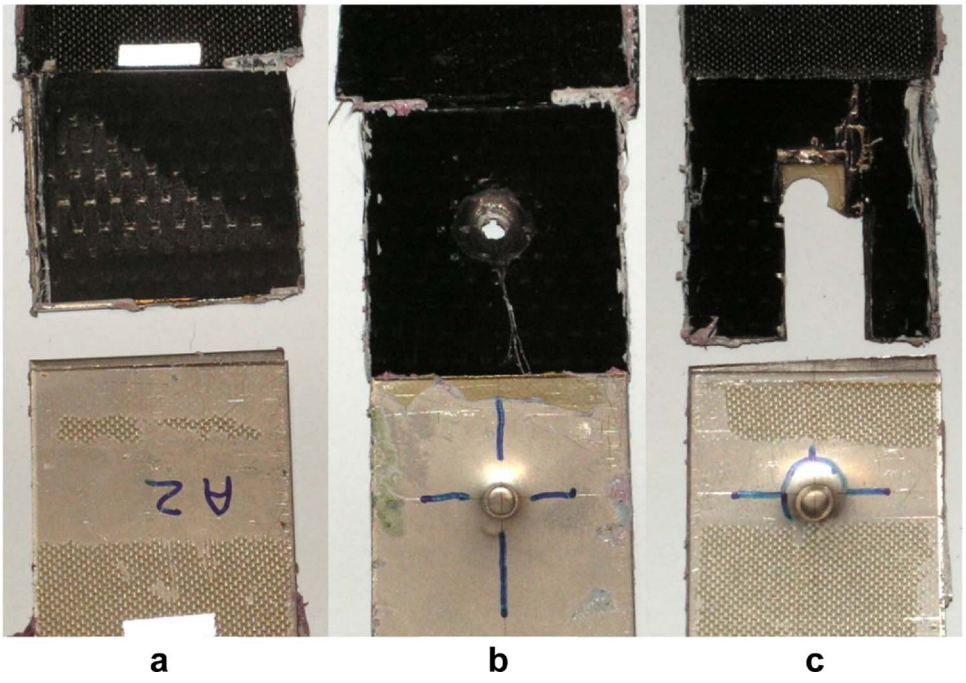

Fig. 11. Photographs of typical joint failure for the: (a) adhesive joint; (b) weld (fibres): (c) weld (no fibres).

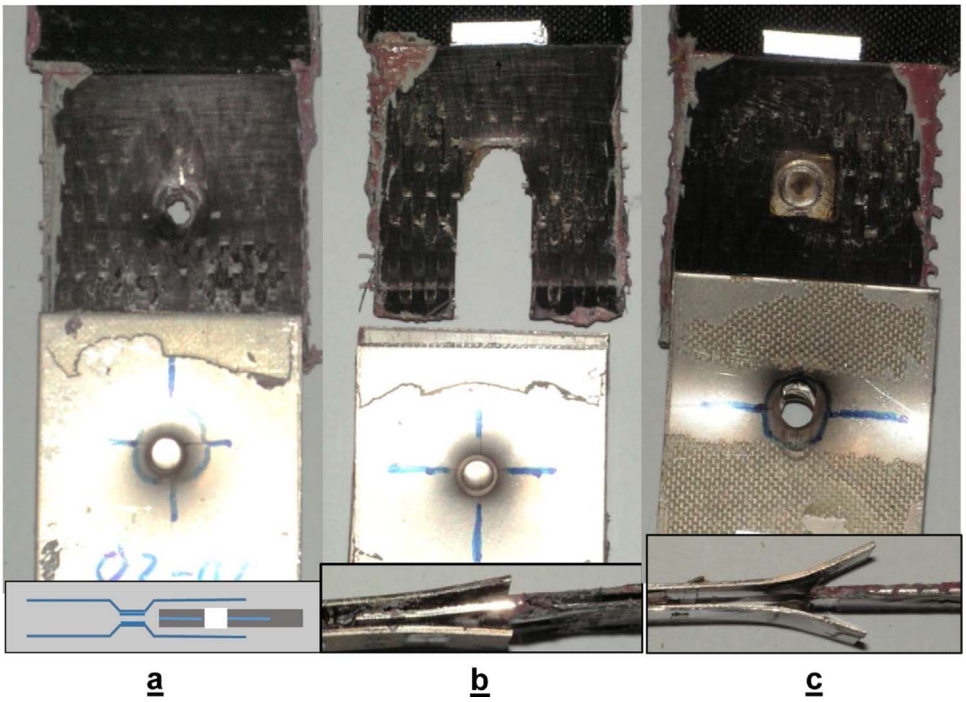

Fig. 12. Photographs of failure for bonded/welded joints (inset illustrates edge perspective of joint failure): (a) weld (fibres) and adhesive; (b) weld (no fibres) and adhesive, composite shear out failure, and weld remained intact; (c) weld (no fibres) and adhesive, weld nugget torn from steel adherends.

graphitised in tetragonal form which is characteristic of polycrystalline graphite formed under heavy deforming forces or as flakes. Graphitisation is normal given the carbon concentration and also presence of nickel in the stainless steel which helps this to occur. There are also traces of carbide, most likely chromium carbides or complex carbide based on chromium and manganese shown in area (i) within Fig. 8(d). In addition, molten metal escapes from the weld nugget formation region and flows along the direction of the carbon fibre. This is observable in the macrosection displayed in Fig. 9, indicating interactions between molten metal, carbon fibre, and metal substrate are not confined to the point where the resistance spot weld is applied. Direct joining of carbon fibre and metal contributes to the overall performance of the reinforced adhesive joint. Singh et al. (2007, 2005) demonstrated that Braze joining is an effective means of joining metals and ceramic matrix composites. Further investigation of this 'braze-joining', which may be occurring in the fibre penetrating RSW joints, could be quantified by fibre pull-out tests. If braze-joining were proven to be an advantage to the overall joining mechanism the manufacturing method could be developed to generate a greater quantity of weld splash.

3.3. Joint performance

Fig. 10 provides baseline data for the joint performance and strength, and the failure mechanisms for these joints are summarised in Table 3. The adhesive joint failure starts at very low strain, which is most likely to be initiated by out-of-plane peel and the joint finally fails

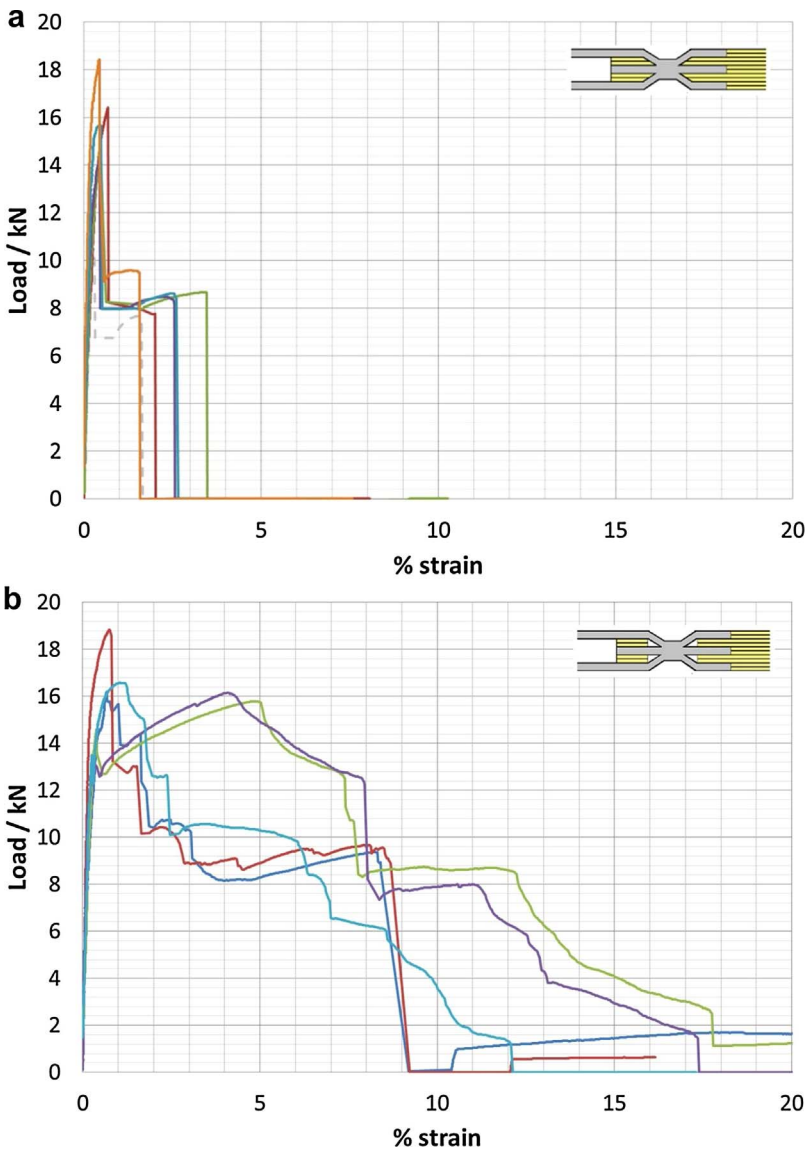

Fig. 13. Plots of the load vs. strain curves for (a) weld (fibres) and adhesive bond and (b) weld (no fibres) and adhesive bond.

when the shear loading on the remaining length of lap joint causes cohesive failure of the adhesive (Fig. 11(a)). Variation in adhesive bond quality results in a wide variation of failure loads.

The weld-only joint strengths depended on whether the joints were made with or without the carbon fibres. Welding through the fibres created an inferior joint which failed with a relatively low load (Fig. 10) due to embrittlement from the carbon in the fibres (Callister and Rethwisch, 2015), leaving the composite adherend intact (Fig. 11(b)). This contrasts with the joint without fibres which had much greater strength (Fig. 10), and caused composite shear-out while the weld remained intact (Fig. 11(c)).

The remaining 3 joint configurations demonstrated more complex failure modes with all exhibiting some degree of improved performance, Fig. 10. Combining the adhesive and weld created a stronger joint. One reason is the weld may reduce the peel stress acting on the steel adherend run-outs, for both types of welded/adhesive joints. This delays initial failure of the adhesive component and results in an increase in maximum load. Alternatively the splash from the weld nugget may provide a braze joint with the fibres which improves strength (see previous section).

The characteristic load/strain curves for the bonded/welded joints of interest are presented in Fig. 13. For the joints where the weld was applied through the carbon fibres, the behaviour of all 5 test specimens was essentially identical. The weld acted to reinforce the adhesive joint, increasing the observed load to failure from 10.3 kN to 15.8 kN. When the adhesive bond failed, a sharp load drop occurred as load was transferred to the weld nugget. The remaining welded joint was not able to support increased loads and the joint deformed at almost constant (reduced) load until the weld fractured (Fig. 12(a)). Strain to failure is limited by the brittle nature of the weld nugget due to carbon contamination.

The behaviour of the joints without carbon fibres were more varied. Joint failure occurred by one of two mechanisms: two of the five specimens achieved maximum load at a strain of around 1%, at which point the adhesive bond failed and the load was transferred wholly to the weld nugget (Fig. 12(b)). Further loading of the joint caused shear-out of the composite adherend similar to that observed with the simple welded (no fibres) joint, Fig. 11(b). Two specimens exhibited initial failure of the adhesive bond at loads less than 14 kN, but the joints were still able to support load increases up to 16 kN at approximately 5% strain. At 8% strain the characteristic load drop associated with complete adhesive bond failure was recorded. The weld then carried a reduced load until complete failure at strains greater than 15%. At complete failure these two samples had the composite adherend still intact (no shear-out) and adhesively bonded to the steel centre insert (Fig. 12(c)). The weld had failed by ductile tearing of the weld nugget

from the steel outer adherends. The remaining sample failed in a similar manner but without the distinctive load maximum at 5% strain. Further development of the process would need to isolate the precise cause of the different failure modes to ensure that the most favourable type (second) consistently occurs.

The bonded/bolted joint fails at loads less than the simple bonded joint and this indicates that the bolt does not act to either carry any significant load or reduce the out-of-plane peel stress. Although the bolt does not increase the joint strength, it provides residual strength and increases the strain to failure. The reduction in strength relative to the 'adhesive only' joint is attributed to either the reduced bond area or damage caused by drilling. In addition, although the bolt was selected to have the same area as the weld nuggets, the welds produced significant amounts of splash (see previous section) which allowed brazing between the molten metal and fibres which could have enhanced joint strength. Finally, the clamping load provided by the resistance spot weld could have been larger than that provided by the bolt reducing the peel stresses.

Overall, the joint with the greatest mechanical performance is the weld (no fibres) reinforced adhesive joint, although even the weld where the fibres are present performs well and is superior to the bolted joint in terms of strength. When comparing the two joint types, if strength is the prime concern for the structural application then there is no need to perform the pre-processing operation of cutting holes in fabric for resistance spot welding. Eliminating this production step will result in a significantly cheaper joint.

4. Conclusions

- The application of a resistance spot weld prior to adhesive bonding improves joining performance; both in terms of an increase in strength of the adhesive bond and also a reduction in the variability of achieved strengths;
- When forming a carbon fabric penetrating metallic resistance spot weld the electrode pinch force is the parameter that has greatest effect; influencing both the through-thickness electrical resistance and also the quality of subsequent weld nugget formation. Further improvements to the process may be possible with equipment that can apply a higher pinch force.
- The strength of resistance spot welded reinforced adhesive joints is largely independent of whether the fibres are present prior to making the resistance spot weld, however the strain to failure is significantly better for the joints where the fibres are removed prior to welding.

Acknowledgements

The authors would like to gratefully acknowledge funding from EPSRC through the Cranfield University Innovative Manufacturing Research Centre (IMRC153) project "Bridging the Divide", as well as Airbus for their financial contribution to the work. In addition, the technical assistance of Fleming Nielson, Brian Brooks, Jim Hurley, and Andrew Dyer, was greatly appreciated.

References

Al-Samhan, A., Darwish, S.M.H., 2003. Finite element modeling of weld-bonded joints. J. Mater. Process. Technol. 142. http://dx.doi.org/10.1016/S0924-0136(02)01015-4.

Berger, L., 2010. Design and fabrication of a structural composite automotive underbody. In: Society of Plastics Engineers − 10th Annual Automotive Composites Conference and Exhibition. Troy, Michigan. pp. 494–503.

Breto, R., Chiminelli, A., Duvivier, E., Lizaranzu, M., Jiménez, M.A., 2015. Finite element analysis of functionally graded bond-lines for metal/composite joints. J. Adhes. 91. http://dx.doi.org/10.1080/00218464.2014.976335.

Callister, W.D., Rethwisch, D.G., 2015. Materials Science and Engineering, 9th ed. John Wiley & Sons.

Darwish, S.M.H., Ghanya, A., 2000. Critical assessment of weld-bonded technologies. J. Mater. Process. Technol. 105, 221–229.

Iijima, S., 1980. Direct observation of the tetrahedral bonding in graphitized carbon black by high resolution electron microscopy. J. Cryst. Growth 50, 675–683. http://dx.doi.org/10.1016/0022-0248(80)90013-5.

Joesbury, A., 2016. New Approaches to Composite Metal Joining. Cranfield University.

Li, L., Sun, L., 2014. Failure mechanisms of Weld bonded lap joints between composite/metal adherends. ASME International Mechanical Engineering Congress and Exposition, Proceedings (IMECE). http://dx.doi.org/10.1115/imece2014-37333.

Nguyen, A.T.T., Amarasinghe, C.K., Brandt, M., Feih, S., Orifici, A.C., 2017. Loading, support and geometry effects for pin-reinforced hybrid metal-composite joints. Compos. Part A Appl. Sci. Manuf. 98. http://dx.doi.org/10.1016/j.compositesa.2017.03.019.

Santos, I.O., Zhang, W., Gonçalves, V.M., Bay, N., Martins, P.A.F., 2004. Weld bonding of stainless steel. Int. J. Mach. Tools Manuf. 44, 1431–1439.

Schwartz, M.M., 1979. Metals Joining Manual.

Shah, B., Frame, B., Dove, C., Fuchs, H., 2010. Structural performance evaluation of composite-to-steel weld bonded joint. In: Society of Plastics Engineers − 10th Annual Automotive Composites Conference and Exhibition 2010. ACCE 2010. pp. 545–561.

Singh, M., Shpargel, T.P., Morscher, G.N., Asthana, R., 2005. Active metal brazing and characterization of brazed joints in titanium to carbon–carbon composites. Int. Conf. Recent Adv. Compos. Mater. 412, 123–128. http://dx.doi.org/10.1016/j.msea.2005.08.179.

Singh, M., Asthana, R., Shpargel, T.P., 2007. Brazing of carbon–carbon composites to Cu-clad molybdenum for thermal management applications. Mater. Sci. Eng. A 452–453, 699–704. http://dx.doi.org/10.1016/j.msea.2006.11.031.

Ucsnik, S., Scheerer, M., Zaremba, S., Pahr, D.H., 2010. Experimental investigation of a novel hybrid metal-composite joining technology. Compos. Part A Appl. Sci. Manuf. 41. http://dx.doi.org/10.1016/j.compositesa.2009.11.003.

Zhang, H., Wen, W., Cui, H., 2012. Study on the strength prediction model of Comeld composites joints. Compos. Part B Eng. 43. http://dx.doi.org/10.1016/j.compositesb.2012.01.085.

2017-08-24

Weld-bonded stainless steel to carbon fibre-reinforced plastic joints

Joesbury, Adam

Elsevier

Joesbury AM, Colegrove PA, Van Rymenant P, et al., (2018) Weld-bonded stainless steel to carbon fibre-reinforced plastic joints. Journal of Materials Processing Technology, Volume 251, January 2018, pp. 241-250

http://dx.doi.org/10.1016/j.jmatprotec.2017.08.023